

Stability of coreless vortices in ferromagnetic spinor Bose-Einstein condensates

V. Pietilä,¹ M. Möttönen,^{1,2} and S. M. M. Virtanen¹

¹Laboratory of Physics, Helsinki University of Technology, P.O. Box 4100, FI-02015 TKK, Finland.

²Low Temperature Laboratory, Helsinki University of Technology, P.O. Box 3500, FI-02015 TKK, Finland.

(Dated: October 30, 2018)

We study the energetic and dynamic stability of coreless vortices in nonrotated spin-1 Bose-Einstein condensates, trapped with a three-dimensional optical potential and a Ioffe-Pritchard field. The stability of stationary vortex states is investigated by solving the corresponding Bogoliubov equations. We show that the quasiparticle excitations corresponding to axisymmetric stationary states can be taken to be eigenstates of angular momentum in the axial direction. Our results show that coreless vortex states can occur as local or global minima of the condensate energy or become energetically or dynamically unstable depending on the parameters of the Ioffe-Pritchard field. The experimentally most relevant coreless vortex state containing a doubly quantized vortex in one of the hyperfine spin components turned out to have very non-trivial stability regions, and especially a quasiperiodic dynamic instability region which corresponds to splitting of the doubly quantized vortex.

PACS numbers: 03.75.Mn, 03.75.Kk, 67.57.Fg

I. INTRODUCTION

Development of optical trapping techniques for alkali atoms has enabled experimental studies of dilute atomic Bose-Einstein condensates (BECs) with spin degrees of freedom [1, 2]. For these systems, the order parameter is a spinor field which can exhibit a rich variety of different topological textures ranging from coreless vortices [3, 4] to monopoles [5, 6] and Skyrmion-type configurations [7, 8, 9]. In scalar BECs, a vortex is always fully characterized by the phase winding about the vortex core, whereas in spinor BECs the characteristics of a vortex are determined by winding numbers of different components as well as the core polarization – for coreless vortices the superfluid velocity is non-divergent at the vortex core and hence the vortex core can be polarized.

Coreless vortices are topologically unstable, i.e., they can be continuously deformed to a uniform texture. Thus their existence as stable states typically requires the presence of additional forces such as interactions at large distances from the vortex core or external fields which impose nontrivial asymptotic boundary conditions [10, 11]. Coreless vortices such as the Mermin-Ho vortices in spinor BECs are analogous to those in superfluid ³He-A [3], in which they appear as equilibrium objects if the system is rotated externally. Thus it is natural to assume that such objects would be generated also in rotated gaseous condensates. It has indeed been theoretically confirmed that also in these systems the Mermin-Ho vortices are energetically stable for certain values of the trap rotation frequency and magnetization [12].

Manipulating spinor condensates with external magnetic fields has been in vogue among both theorists and experimentalist during the recent years [13, 14, 15, 16, 17]. Topological phase engineering by time-dependent external magnetic fields has been successfully used to

create vortex structures [14, 18, 19, 20, 21]. Recently, Leanhardt *et al.* succeeded in creating a coreless vortex in a $F = 1$ spinor condensate in a Ioffe-Pritchard (IP) magnetic trap [22] by adiabatically switching off the magnetic bias field along the trap axis [15]. The ground state phase diagram corresponding to the IP field combined with an optical confinement potential has been computed for a condensate uniform in the direction of the vortex axis [16], and it shows that the IP field renders the ground state of the system to be a coreless vortex. This is due to the tendency of the spin to align with the external field, which leads to formation of a coreless vortex. An example of the spin texture in an IP field is shown in Fig. 1 in the pancake-shaped geometry of Ref. [16]. Zhang *et al.* [17] found that within an adiabatic approximation [13], the difference of atomic spatial angular momentum and hyperfine spin is conserved in the IP field. This conservation law implies that the ground state of the condensate carries a persistent current with definite winding numbers.

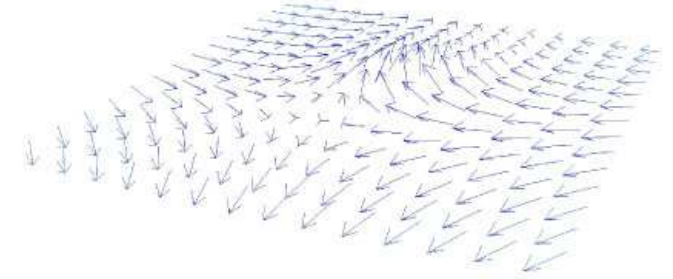


FIG. 1: (Color online) One possible spin texture of a coreless vortex in pancake-shaped condensate in the presence of the Ioffe-Pritchard field. Spin of the condensate tends to align with the external field.

In the previous studies [16, 17] only the global energetic stability of coreless vortex states was considered. How-

ever, the coreless vortices created in the experiment [15] contain a doubly quantized vortex in one of the hyperfine spin states, and it is of interest to find out whether such coreless vortex states inherit the dynamic instability of doubly quantized vortices in scalar condensates [23, 24, 25, 26, 27, 28]. Furthermore, the topological phase imprinting methods [14, 18, 19, 20, 21] used to create doubly quantized vortices involve adiabatic inversion of the bias field in the presence of the IP field. The intermediate state in this process is always a coreless vortex which for certain field parameters is the ground state of the system but otherwise its stability properties are so far unknown. Hence the study of stability of coreless vortices can also give valuable insight to the process of vortex creation using topological phase engineering.

In this paper, we analyze further the vortex stability phase diagram of ferromagnetic spinor condensates in the presence of a IP field and an optical trap potential by computing the quasiparticle spectra from the Bogoliubov equations in finite three-dimensional trap geometries, for oblate, spherical, and prolate condensates. We show that different coreless vortex states are locally energetically stable for a wide range of IP field configurations, although for other parameter values dynamic and energetic instabilities may occur. Quasiparticle states corresponding to these instabilities reveal that the dynamic instability of coreless vortices containing doubly quantized vortices in one of the hyperfine spin components is similar to the dynamic instability of the doubly quantized vortices in scalar condensates, that is, the doubly quantized vortices tend to split due to the instability.

II. MEAN FIELD THEORY

In the mean-field approximation, we describe the condensate formed by weakly interacting ultra-cold bosonic atoms in the z -quantized basis $|F = 1, m_F\rangle$, $m_F = -1, 0, 1$, with a spinor field $\psi = (\psi_1 \ \psi_0 \ \psi_{-1})^T$ and the free energy functional of the form [3, 4]

$$\mathcal{E}[\psi] = \int d\mathbf{r} \left[\frac{\hbar^2}{2m} |\nabla\psi(\mathbf{r})|^2 + U(\mathbf{r})|\psi(\mathbf{r})|^2 - \mu|\psi(\mathbf{r})|^2 + \frac{c_0}{2} |\psi(\mathbf{r})|^4 + \frac{c_2}{2} |\mathbf{S}(\mathbf{r})|^2 \right], \quad (1)$$

where the spin density is given by

$$\mathbf{S}(\mathbf{r}) = \sum_{a,b} \psi_a^*(\mathbf{r}) \mathbf{F}_{ab} \psi_b(\mathbf{r}), \quad (2)$$

and the angular momentum matrices $\mathbf{F} = (F_x \ F_y \ F_z)^T$ are the usual generators of the spin rotation group $SO(3)$ with matrix representations

$$F_x = \frac{1}{\sqrt{2}} \begin{pmatrix} 0 & 1 & 0 \\ 1 & 0 & 1 \\ 0 & 1 & 0 \end{pmatrix}, \quad F_y = \frac{i}{\sqrt{2}} \begin{pmatrix} 0 & -1 & 0 \\ 1 & 0 & -1 \\ 0 & 1 & 0 \end{pmatrix}, \quad F_z = \begin{pmatrix} 1 & 0 & 0 \\ 0 & 0 & 0 \\ 0 & 0 & -1 \end{pmatrix}. \quad \mathcal{D} = \begin{pmatrix} A & -B \\ B^* & -A^* \end{pmatrix},$$

Above, m is the mass of the atoms, μ the chemical potential, and c_0, c_2 are the coupling constants related to s -wave scattering lengths in different total hyperfine spin channels [3]. Depending on whether the interaction coupling constant c_2 is positive or negative, the condensate is either antiferromagnetic or ferromagnetic, respectively. Klausen *et al.* [29] have shown that ^{87}Rb is ferromagnetic, whereas ^{23}Na atoms realize an antiferromagnetic condensate [30]. We take the confining potential $U(\mathbf{r})$ created by an external optical field to be the axisymmetric harmonic potential

$$U(\mathbf{r}) = \frac{1}{2}(\omega_r^2 r^2 + \omega_z^2 z^2) = \frac{\omega_r^2}{2}(r^2 + \lambda^2 z^2),$$

where $\lambda = \omega_z/\omega_r$.

In the presence of an additional external magnetic field $\mathbf{B}(\mathbf{r})$, we take also into account the linear Zeeman term $\mu_B g_F \mathbf{B}(\mathbf{r}) \cdot \mathbf{S}(\mathbf{r})$ in the energy functional. The constant μ_B is the Bohr magneton and g_F is the Landé g -factor. The free energy becomes in this case

$$\mathcal{F}[\psi] = \mathcal{E}[\psi] + \mu_B g_F \int d\mathbf{r} \mathbf{B}(\mathbf{r}) \cdot \mathbf{S}(\mathbf{r}), \quad (3)$$

and the magnetic field is in our analysis of the Ioffe-Pritchard form

$$\mathbf{B}(\mathbf{r}) = B_\perp(x\hat{\mathbf{x}} - y\hat{\mathbf{y}}) + B_z\hat{\mathbf{z}}.$$

Stationary states of the condensate satisfy $\delta\mathcal{F}[\psi]/\delta\psi = 0$, which yields the Gross-Pitaevskii (GP) equation

$$\mathcal{H}[\psi]\psi = \mu\psi, \quad (4)$$

where the non-linear operator $\mathcal{H}[\psi]$ is given by

$$\mathcal{H}[\psi] = -\frac{\hbar^2}{2m}\nabla^2 + U(\mathbf{r}) + \mu_B g_F \mathbf{B}(\mathbf{r}) \cdot \mathbf{F} + c_0|\psi(\mathbf{r})|^2 + c_2 \mathbf{F} \cdot \mathbf{S}(\mathbf{r}).$$

The quasiparticle spectrum corresponding to a given stationary state can be solved from the generalized Bogoliubov equations [12, 31]

$$\mathcal{D} \begin{pmatrix} u_q(\mathbf{r}) \\ v_q(\mathbf{r}) \end{pmatrix} = \hbar\omega_q \begin{pmatrix} u_q(\mathbf{r}) \\ v_q(\mathbf{r}) \end{pmatrix}, \quad (5)$$

where $u_q = (u_{q,1} \ u_{q,0} \ u_{q,-1})^T$ and $v_q = (v_{q,1} \ v_{q,0} \ v_{q,-1})^T$ are the quasiparticle amplitudes and the operator \mathcal{D} is defined as

such that the components of the A and B operators are

$$\begin{aligned}
A_{ij} = & \left(-\frac{\hbar^2}{2m} \nabla^2 + U(\mathbf{r}) - \mu \right) \delta_{ij} + \mu_B g_F \sum_{\alpha} B_{\alpha}(\mathbf{r}) (F_{\alpha})_{ij} \\
& + c_0 \left\{ \sum_k |\psi_k(\mathbf{r})|^2 \delta_{ij} + \psi_i(\mathbf{r}) \psi_j^*(\mathbf{r}) \right\} \\
& + c_2 \sum_{\alpha} \sum_{k,l} [(F_{\alpha})_{ij} (F_{\alpha})_{kl} + (F_{\alpha})_{il} (F_{\alpha})_{kj}] \psi_k^*(\mathbf{r}) \psi_l(\mathbf{r}), \\
B_{ij} = & c_0 \psi_i(\mathbf{r}) \psi_j(\mathbf{r}) + c_2 \sum_{\alpha} \sum_{k,l} (F_{\alpha})_{ik} (F_{\alpha})_{jl} \psi_k(\mathbf{r}) \psi_l(\mathbf{r}),
\end{aligned}$$

for $i, j \in \{1, 0, -1\}$. Due to the conjugate symmetry of the Bogoliubov equations, we may concentrate only on the quasiparticle modes for which the quadratic form $\int d\mathbf{r} (|u_q(\mathbf{r})|^2 - |v_q(\mathbf{r})|^2)$ is non-negative. The quasiparticle spectrum determines the stability properties of the corresponding stationary state: If the quasiparticle spectrum contains excitations with non-real frequencies ω_q , the system is dynamically unstable and even small initial perturbations can render the population of these modes to grow exponentially in time even in the absence of dissipation. On the other hand, if there exists modes with negative eigenfrequencies, the state is energetically unstable, and in the presence of dissipation the condensate can lower its energy by transferring particles from the condensate state to such anomalous modes. Vice versa, if all the quasiparticle eigenfrequencies are positive, the state is locally energetically and dynamically stable, and should be long-living and robust against small perturbations even in the presence of dissipational mechanisms.

III. AXISYMMETRIC VORTEX STATES

Within an adiabatic approximation, that is, assuming that hyperfine spins of the atoms remain aligned (or antialigned) with the local magnetic field, the ground state of the condensate in the IP field is axisymmetric [17]. However, nonadiabatic effects are important to some extent, since in Ref. [16] the ground state phase diagram was shown to contain a non-axisymmetric vortex state in the antiferromagnetic case. On the other hand, we have verified with fully three-dimensional (3D) computations, i.e. without setting any symmetry restrictions to the condensate wavefunction, that for ferromagnetic condensates with nonzero radial IP field strength, the ground state is always axisymmetric for all the parameter values considered. Consequently, we restrict to consider only configurations that are axisymmetric.

In cylindrical coordinates $\mathbf{r} = (r, \varphi, z)$, axially symmetric vortex states are of the form

$$\psi(\mathbf{r}) = (\psi_1(r, z) e^{i\kappa_1 \varphi} \quad \psi_0(r, z) e^{i\kappa_0 \varphi} \quad \psi_{-1}(r, z) e^{i\kappa_{-1} \varphi})^T, \quad (6)$$

where $\kappa_i \in \mathbb{Z}$ are the winding numbers of the three components—we refer to states of this form as

$\langle \kappa_1, \kappa_0, \kappa_{-1} \rangle$. In addition, all physically measurable densities corresponding to axisymmetric states have to be axisymmetric. When applied to spin-density, this requirement combined with Eqs. (2) and (6) implies the relation

$$2\kappa_0 = \kappa_1 + \kappa_{-1}, \quad (7)$$

between the winding numbers. The angular dependence of the IP field sets additional restrictions for the ground state to be axisymmetric: For the Zeeman energy term $\mu_B g_F \mathbf{B}(\mathbf{r}) \cdot \mathbf{S}(\mathbf{r})$ to be rotationally symmetric the winding numbers of the condensate state have to satisfy the additional constraints

$$\kappa_0 = \kappa_1 - 1 = \kappa_{-1} + 1. \quad (8)$$

One notes that these latter relations imply also the relation in Eq. (7), and are thus more restrictive. We have verified with fully 3D computations without any symmetry assumptions that the ground state of system indeed satisfies the restrictions given in the Eqs. (6)–(8). The states with the lowest angular momenta satisfying Eqs. (7) and (8) are $\langle 2, 1, 0 \rangle$, $\langle 1, 0, -1 \rangle$, and $\langle 0, -1, -2 \rangle$ which are coreless vortex states. The numerical results indeed show that the ground state in the presence of a strong enough IP field contains a coreless vortex.

The coreless vortices in the states $\langle 2, 1, 0 \rangle$ and $\langle 0, -1, -2 \rangle$ are ferromagnetic in the sense that the spin of the condensate is aligned (or antialigned) with the external field also in the core region. Furthermore, $\langle 2, 1, 0 \rangle$ and $\langle 0, -1, -2 \rangle$ are equivalent since they differ only by inversion of the spin quantization axis. On the other hand, $\langle 1, 0, -1 \rangle$ is polar in the sense that at the vortex core $\mathbf{S}(\mathbf{r})$ vanishes [3, 31]. The difference in the spin texture turns out to be significant for the phase diagram and the local energetic stability of the vortex state. Due to vanishing spin density at the vortex core, the spin texture of the polar vortex $\langle 1, 0, -1 \rangle$ can align with the IP field equally well for both positive and negative values of the bias field B_z .

In investigating the stability properties of stationary states by solving the Bogoliubov equations, it is to be noted that apart from the possible degeneracy of spectrum, axisymmetric states can have non-axisymmetric quasiparticle excitations also due to the fact that \mathcal{D} does not in general commute with the angular momentum operator $\hat{L}_z = -i\hbar \partial_{\varphi}$. We can, however, show that if the winding numbers of different components satisfy Eq. (8), then there exists a unitary transformation \mathcal{U} such that the transformed Bogoliubov operator $\tilde{\mathcal{D}} = \mathcal{U}^{\dagger} \mathcal{D} \mathcal{U}$ commutes with \hat{L}_z . The unitary transformation \mathcal{U} is in this case given by

$$\mathcal{U} = \begin{pmatrix} \mathcal{U}_0 & 0 \\ 0 & \mathcal{U}_0^{\dagger} \end{pmatrix}, \quad \text{where } \mathcal{U}_0 = \begin{pmatrix} e^{i\kappa_1 \varphi} & 0 & 0 \\ 0 & e^{i\kappa_0 \varphi} & 0 \\ 0 & 0 & e^{i\kappa_{-1} \varphi} \end{pmatrix},$$

for the Bogoliubov operator $\mathcal{D} = \mathcal{D}[\psi]$ corresponding to an axisymmetric state $\langle \kappa_1, \kappa_0, \kappa_{-1} \rangle$. Now $[\tilde{\mathcal{D}}, \hat{L}_z] = 0$

follows from the condition stated in Eq. (8). Hence the eigenstates of \tilde{D} can be chosen to be eigenstates of \hat{L}_z . Writing the eigenvalue equation $\tilde{D}w = \eta w$ in the form $\mathcal{U}\tilde{D}\mathcal{U}^\dagger w = \eta w$ and taking into account that $\mathcal{U}\tilde{D}\mathcal{U}^\dagger = \mathcal{D}$, we observe that the quasiparticle amplitudes in the original Bogoliubov equation (5) can be taken to be of the form

$$u_{q,j}(\mathbf{r}) = u_{q,j}(r, z)e^{i(\kappa_q + \kappa_j)\varphi}, \quad (9)$$

$$v_{q,j}(\mathbf{r}) = v_{q,j}(r, z)e^{i(\kappa_q - \kappa_j)\varphi}, \quad j = -1, 0, 1, \quad (10)$$

where κ_q is an angular momentum quantum number of the excitation. In addition to this analytical argument, we have verified numerically without any symmetry assumptions that for the pancake-shaped condensates with $\lambda = \omega_z/\omega_r \gg 1$, all the low-energy quasiparticle states are axisymmetric.

IV. NUMERICAL RESULTS

In the following we consider ferromagnetic condensates which can be realized, e.g., with ^{87}Rb atoms. For the scattering lengths of ^{87}Rb , the estimate of van Kempen *et al.* [32] implies the ratio $c_2/c_0 \sim -0.005$. In this study we use the value $c_2/c_0 = -0.02$ which was also used in the previous theoretical studies of Mizushima *et al.* [12, 33]. In the numerical calculation we use dimensionless units in which $\tilde{c}_0 = c_0 m N / a_r \hbar$, where the characteristic length scale of the trap is given by $a_r = \sqrt{\hbar/m\omega_r}$. We adopt $\tilde{c}_0 = 10000$, which corresponds, for example, a condensate of $N = 8.5 \times 10^5$ ^{87}Rb atoms trapped such that $\omega_r = 2\pi \times 200$ Hz. We take the Landé g -factor to be $g_F = -\frac{1}{2}$ which indicates that the hyperfine spine tends to align with an external field. We have searched for solutions of the GP equation and the Bogoliubov equations by using finite-difference discretization combined with relaxation methods and the implicitly restarted Arnoldi method implemented in the ARPACK numerical library [34]. In the numerical calculations, we also use the conjugate symmetry of the Bogoliubov equations and consider only positive κ_q , which slightly reduces the numerical effort.

Numerical computations showed that the ground state configuration for non-vanishing perpendicular IP field B_\perp is always one of the coreless vortex states $\langle 2, 1, 0 \rangle$, $\langle 1, 0, -1 \rangle$ or $\langle 0, -1, -2 \rangle$. Figure 2 shows the computed stability phase diagrams displaying the dynamic and energetic stability/instability regions for the state $\langle 2, 1, 0 \rangle$ as a function of the IP field parameters. The corresponding phase diagram for the state $\langle 1, 0, -1 \rangle$ is shown in Fig. 3. The results have been computed for the trap asymmetry parameter values $\lambda = 0.2, 1.0$, and 5.0 , corresponding to prolate, spherical, and oblate geometries, respectively. The phase diagram for the state $\langle 0, -1, -2 \rangle$ is the same as for $\langle 2, 1, 0 \rangle$ if the sign of the bias field B_z is reversed.

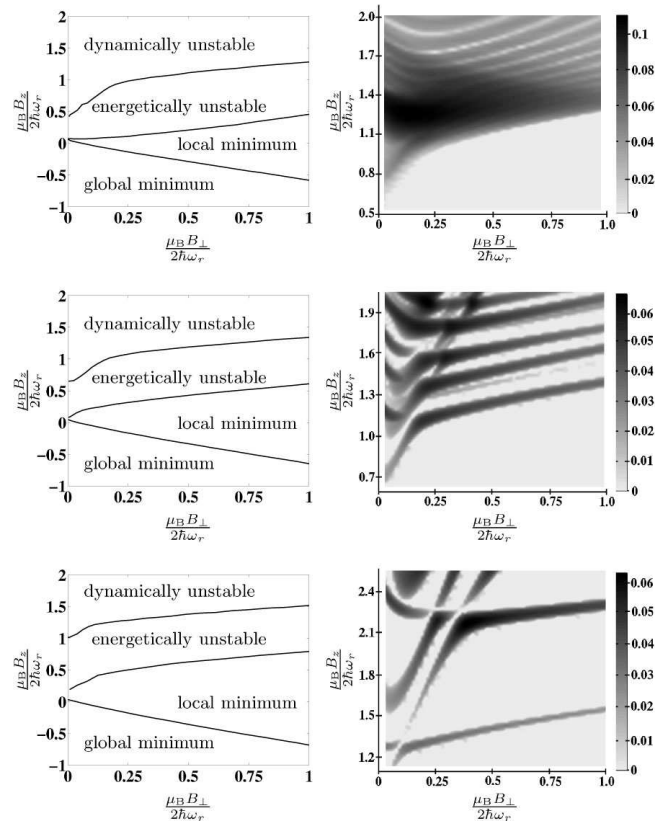


FIG. 2: Stability phase diagram for the axially symmetric $\langle 2, 1, 0 \rangle$ vortex state. On the top $\lambda = 0.2$, in the middle $\lambda = 1.0$, and at the bottom $\lambda = 5.0$. The left panels show the different stability phases and the right panels the maximum value of $|\text{Im}\{\omega_q/\omega_r\}|$ for each point in the (B_\perp, B_z) plane as a grayscale plot: bright regions correspond to dynamically stable regions, and dark ones dynamically unstable. In the region denoted as “local minimum” $\langle 2, 1, 0 \rangle$ is a local minimum of the mean field energy and the polar state $\langle 1, 0, -1 \rangle$ is the ground state of the system. The dynamic instability region indicates the section of the parameter space where dynamic instability modes can appear.

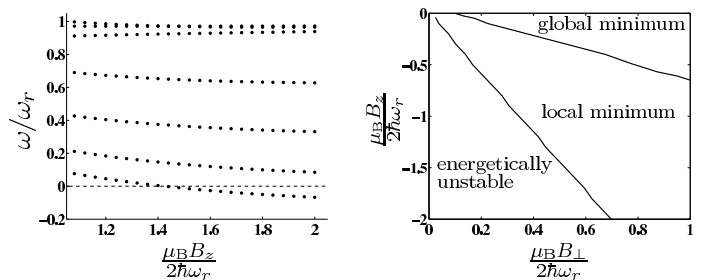


FIG. 3: Stability phase diagram of the polar vortex $\langle 1, 0, -1 \rangle$ (right panel) and the lowest energy excitations as a function of B_z for fixed $\mu_B B_\perp / 2\hbar\omega_r = 0.5$ (left panel). The phase diagram is symmetric with respect to reversing the sign of B_z .

From the diagrams one infers that the ferromagnetic

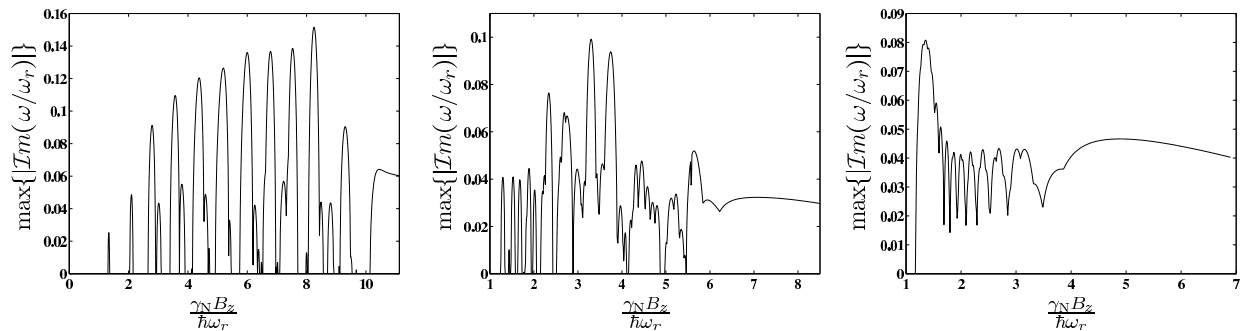


FIG. 4: Quasiperiodic structure of the dynamic instability as a function of B_z for the axially symmetric $\langle 2, 1, 0 \rangle$ vortex and $\frac{\mu_B B_\perp}{2\hbar\omega_r} = 0.7$. Left panel: $\lambda = 5.0$; middle: $\lambda = 1.0$; and right panel: $\lambda = 0.2$.

state $\langle 2, 1, 0 \rangle$ and the polar state $\langle 1, 0, -1 \rangle$ can co-exist as local energy minima for suitable IP field parameters. The transition between the ferromagnetic and polar ground states is determined by the relative magnitude of the IP field components: for $B_\perp \gg |B_z|$ the ferromagnetic core of the vortex states $\langle 2, 1, 0 \rangle$ and $\langle 0, -1, -2 \rangle$ becomes energetically unfavorable, rendering the polar state $\langle 1, 0, -1 \rangle$ the global minimum of energy, and vice versa for $|B_z| \gg B_\perp$.

The negative energy anomalous modes indicating energetic instability occur for quantum numbers $\kappa_q = \pm 1$ for the polar state $\langle 1, 0, -1 \rangle$ and for $\kappa_q = \pm 2$ for the ferromagnetic state $\langle 2, 1, 0 \rangle$. The $\langle 1, 0, -1 \rangle$ state turned out to be dynamically stable for all the parameter values investigated, but the states $\langle 2, 1, 0 \rangle$ and $\langle 0, -1, -2 \rangle$ have complicated dynamic instability regions. The dynamic instability modes occur only for $\kappa_q = \pm 2$. Figure 2 shows the greyscale plots of the maximum imaginary parts of the Bogoliubov eigenfrequencies for the state $\langle 2, 1, 0 \rangle$ as functions of the IP field parameters for three trap geometries. We note that the regions marked as dynamically unstable in Fig. 2 contain narrow stripe-like patterns in which the vortex state is in fact dynamically stable. However, especially for the prolate geometry these stripes are very narrow and probably experimentally indistinguishable. The stripe-like quasiperiodic structure of the dynamic instability can be observed more clearly in Fig. 4, in which the maximum imaginary part is plotted for a fixed value of B_\perp . One observes that the magnitude of the largest imaginary part oscillates markedly before it saturates for strong enough bias fields B_z .

Figure 2 shows that the $\langle 2, 1, 0 \rangle$ vortex tends to become dynamically more stable with increasing λ , i.e., the vortex is generally more stable in the pancake shaped geometry than in the cigar shaped one. This is due to the suppression of the density of low-energy excitations in the limit of tight confinement in the z direction. However, the dynamic instability persists even for $\lambda = \omega_z/\omega_r \gg 1$. The energetic stability of the coreless vortices is intimately related to dynamic instability since it has been shown in Ref. [28] that dynamic instabilities in scalar condensates are formed when a negative and a

positive energy excitation are in resonance. Similar phenomenon takes place also in spinor condensates, and can be observed in this case by inspecting the spectrum of the quasiparticle energies for $\kappa_q = \pm 2$ shown in Fig. 5. For $\lambda = 1.0$ and $\mu_B B_\perp/2\hbar\omega_r = 0.5$, the dynamic instability may occur for parameter values $\mu_B B_z/2\hbar\omega_r \gtrsim 1.16$. From Fig. 5 one observes that some positive energy excitations are missing in the region $\mu_B B_z/2\hbar\omega_r \gtrsim 1.16$ due to the resonance. We note that the regions in which the $\langle 2, 1, 0 \rangle$ vortex is dynamically stable seem to be manifested by the absence of certain positive and negative energy excitations. For the polar vortex $\langle 1, 0, -1 \rangle$ the excitation spectrum is much simpler containing only one anomalous mode. The stability phase diagram for the polar state $\langle 1, 0, -1 \rangle$ in spherical geometry is shown in Fig. 3 together with the lowest quasiparticle energies.

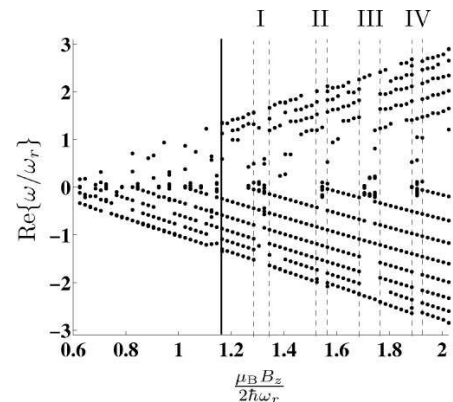


FIG. 5: The negative energy excitations and the corresponding positive energy excitations with $\kappa_q = \pm 2$ for the ferromagnetic vortex state $\langle 2, 1, 0 \rangle$. Here $\mu_B B_\perp/2\hbar\omega_r = 0.5$ and $\lambda = 1.0$ are fixed. The dynamic instabilities start to occur for $\mu_B B_z/2\hbar\omega_r \gtrsim 1.16$ which is denoted by the solid line. The intervals denoted by the dashed lines and the Roman numerals I, II, III, and IV correspond to regions of values of B_z for which the $\langle 2, 1, 0 \rangle$ vortex state is dynamically stable (cf. Fig. 2).

For the ferromagnetic vortex state $\langle 2, 1, 0 \rangle$, the unit vector field $\hat{\mathbf{n}}(\mathbf{r}) = \mathbf{S}(\mathbf{r})/|\mathbf{S}(\mathbf{r})|$ is well-defined everywhere

inside the cloud. Thus the spin texture of this state can be mapped to a simply connected subset $\mathcal{S} \subset S^2$ and the perpendicular part of the IP field prevents the subset \mathcal{S} from shrinking to a point. The surface \mathcal{S}' corresponding to the spin texture of the polar vortex $\langle 1, 0, -1 \rangle$ contains a hole due to vanishing $\mathbf{S}(\mathbf{r})$ at the vortex core. Thus the two spin textures are topologically inequivalent and there is a topological phase transition of the ground state between the two textures occurring at the boundary between the regions of global and local stability in Fig. 2.

To investigate qualitatively the nature of the dynamic instability, we consider states of the form

$$\tilde{\psi}(\mathbf{r}) = \psi(\mathbf{r}) + \eta[u_q(\mathbf{r}) + v_q^*(\mathbf{r})], \quad (11)$$

where a slightly populated quasiparticle state corresponding to the dynamic instability with the largest imaginary frequency has been added to the corresponding stationary state. Isosurfaces of particle densities in different hyperfine spin components of such slightly perturbed $\langle 2, 1, 0 \rangle$ vortex states are shown in Fig. 6. In the component containing the doubly quantized vortex, one observes a helical vortex chain structure, which is very similar to the one discovered in the numerical calculations of Huhtamäki *et al.* [25] for the splitting times of doubly quantized vortices in scalar condensates. Thus we observe that for the $\langle 2, 1, 0 \rangle$ vortex, the dynamic instability is essentially due to the splitting of the doubly quantized vortex in the $m_F = +1$ component. Due to the helical structure of the splitted vortex in this multicomponent case, the splitting of the doubly quantized vortex is accompanied with a spiral flow about the z -axis of the vortex free component $m_F = -1$.

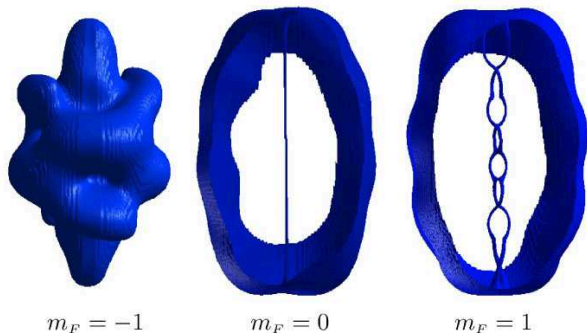


FIG. 6: (Color online) Isosurfaces of particle densities in different spin components corresponding to vortex state $\langle 2, 1, 0 \rangle$ and a slight excitation of a dynamic instability mode. The trap asymmetry parameter is $\lambda = 0.2$. Population of the dynamic instability mode is 1% of the total number of particles. The isosurfaces correspond to values $|\Psi_1(\mathbf{r})|^2 = 2.6 \cdot 10^{-5} N/a_r^3$, $|\Psi_0(\mathbf{r})|^2 = 1.0 \cdot 10^{-5} N/a_r^3$, and $|\Psi_{-1}(\mathbf{r})|^2 = 1.0 \cdot 10^{-5} N/a_r^3$.

Due to the Zeeman energy term, the average spin $\mathbf{S}(\mathbf{r})$ tends to align with the local magnetic field. However, in

the vicinity of the vortex core the average spin may deviate from the direction of the local magnetic field without costing too much energy. The spin texture of the state $\langle 2, 1, 0 \rangle$ outside the vortex core points always along the local magnetic field, but for $B_z > 0$, $\mathbf{S}(\mathbf{r})$ has opposite direction to the magnetic field. Since the perpendicular part of the IP field is topologically nontrivial with winding number -1 [15, 35], a continuous transformation of the spin texture to energetically more favorable state cannot be accomplished without spin rotations against the local magnetic field. Thus the IP field creates an energy barrier which prevents the spin texture from unwinding itself via spin rotations.

V. CONCLUSIONS

In conclusion, we have studied the local stability of coreless vortex states in optically trapped ferromagnetic spinor $F = 1$ BECs in the presence of the Ioffe-Pritchard field. The ground states of the system turned out to be axisymmetric and it was shown analytically that the corresponding quasiparticle states are also axisymmetric. By computing numerically the quasiparticle spectra we have shown that there can co-exist different coreless vortex states as local and global minima of energy for a wide variety of different external field configurations. The experimentally most tractable vortex configuration, the coreless vortex state $\langle 2, 1, 0 \rangle$, was shown to possess a rich phase diagram in which the vortex transforms gradually from a global minimum of energy to a dynamically unstable stationary state as the bias field of the Ioffe-Pritchard trap is ramped up from negative to positive bias. Based on these results one should be able to realize experimentally robust coreless vortex states by loading the atoms into an optical trap with an IP field and allowing the condensate to relax into the ground state. This method should also enable experimental creation of the polar vortex state $\langle 1, 0, -1 \rangle$. Interesting questions for the future research would be to investigate the phase diagram of the ground state and the local stability of vortex states in an external Friedberg-Paul (hexapole) magnetic field [36, 37], and the exact decay mechanisms of energetically unfavorable spin textures.

Acknowledgments

CSC-Scientific Computing Ltd (Espoo, Finland) is acknowledged for computational resources and Academy of Finland for extensive financial support. M.M. thanks Finnish Cultural Foundation, Väisälä Foundation, and Magnus Ehnrooth Foundation for financial support. V.P. thanks the Jenny and Antti Wihuri Foundation for financial support. J.A.M. Huhtamäki is appreciated for stimulating discussions.

-
- [1] D. M. Stamper-Kurn, M. R. Andrews, A. P. Chikkatur, S. Inouye, H.-J. Miesner, J. Stenger, and W. Ketterle, *Phys. Rev. Lett.* **80**, 2027 (1998).
- [2] M. D. Barrett, J. A. Sauer, and M. S. Chapman, *Phys. Rev. Lett.* **87**, 010404 (2001).
- [3] T. L. Ho, *Phys. Rev. Lett.* **81**, 742 (1998).
- [4] T. Ohmi and K. Machida, *J. Phys. Soc. Jpn.* **67**, 1822 (1998).
- [5] H. T. C. Stoof, E. Vliegen, and U. Al Khawaja, *Phys. Rev. Lett.* **87**, 120407 (2001).
- [6] J.-P. Martikainen, A. Collin, and K.-A. Suominen, *Phys. Rev. Lett.* **88**, 090404 (2002).
- [7] U. Al Khawaja and H. T. C. Stoof, *Nature (London)* **411**, 918 (2001).
- [8] U. Al Khawaja and H. T. C. Stoof, *Phys. Rev. A* **64**, 043612 (2001).
- [9] H. Zhai, W. Q. Chen, Z. Xu, and L. Chang, *Phys. Rev. A* **68**, 043602 (2003).
- [10] M. M. Salomaa and G. E. Volovik, *Rev. Mod. Phys.* **59**, 533 (1987).
- [11] D. Vollhardt and P. Wölfle, *The Superfluid Phases of Helium 3* (Taylor and Francis, London, 1990).
- [12] T. Mizushima, K. Machida, and T. Kita, *Phys. Rev. Lett.* **89**, 030401 (2002).
- [13] T. L. Ho and V. B. Shenoy, *Phys. Rev. Lett.* **77**, 2595 (1996).
- [14] A. E. Leanhardt, A. Görlitz, A. P. Chikkatur, D. Kielpinski, Y. Shin, D. E. Pritchard, and W. Ketterle, *Phys. Rev. Lett.* **89**, 190403 (2002).
- [15] A. E. Leanhardt, Y. Shin, D. Kielpinski, D. E. Pritchard, and W. Ketterle, *Phys. Rev. Lett.* **90**, 140403 (2003).
- [16] E. N. Bulgakov and A. F. Sadreev, *Phys. Rev. Lett.* **90**, 200401 (2003).
- [17] P. Zhang, H. H. Jen, C. P. Sun, and L. You, *Phys. Rev. Lett.* **98**, 030403 (2007).
- [18] M. Nakahara, T. Isoshima, K. Machida, S. i. Ogawa, and T. Ohmi, *Physica B* **284**, 17 (2000).
- [19] T. Isoshima, M. Nakahara, T. Ohmi, and K. Machida, *Phys. Rev. A* **61**, 063610 (2000).
- [20] S.-I. Ogawa, M. Möttönen, M. Nakahara, T. Ohmi, and H. Shimada, *Phys. Rev. A* **66**, 013617 (2002).
- [21] M. Möttönen, N. Matsumoto, M. Nakahara, and T. Ohmi, *J. Phys.: Condens. Matter* **14**, 13481 (2002).
- [22] D. E. Pritchard, *Phys. Rev. Lett.* **51**, 1336 (1983).
- [23] H. Pu, C. K. Law, J. H. Eberly, and N. P. Bigelow, *Phys. Rev. A* **59**, 1533 (1999).
- [24] M. Möttönen, T. Mizushima, T. Isoshima, M. M. Salomaa, and K. Machida, *Phys. Rev. A* **68**, 023611 (2003).
- [25] J. A. M. Huhtamäki, M. Möttönen, T. Isoshima, V. Pietilä, and S. M. M. Virtanen, *Phys. Rev. Lett.* **97**, 110406 (2006).
- [26] A. M. Mateo and V. Delgado, *Phys. Rev. Lett.* **97**, 180409 (2006).
- [27] J. A. M. Huhtamäki, M. Möttönen, and S. M. M. Virtanen, *Phys. Rev. A* **74**, 063619 (2006).
- [28] E. Lundh and H. M. Nilsen, *Phys. Rev. A* **74**, 063620 (2006).
- [29] N. N. Klausen, J. L. Bohn, and C. H. Greene, *Phys. Rev. A* **64**, 053602 (2001).
- [30] J. Stenger, S. Inouye, D. M. Stamper-Kurn, H.-J. Miesner, A. P. Chikkatur, and W. Ketterle, *Nature (London)* **396**, 345 (1998).
- [31] T. Isoshima, K. Machida, and T. Ohmi, *J. Phys. Soc. Jpn.* **70**, 1604 (2001).
- [32] E. G. M. van Kempen, S. J. J. M. F. Kokkelmans, D. J. Heinzen, and B. J. Verhaar, *Phys. Rev. Lett.* **88**, 093201 (2002).
- [33] T. Mizushima, K. Machida, and T. Kita, *Phys. Rev. A* **66**, 053610 (2002).
- [34] See the ARPACK homepage, URL www.caam.rice.edu/software/ARPACK/.
- [35] N. D. Mermin, *Rev. Mod. Phys.* **51**, 591 (1979).
- [36] E. A. Hinds and C. Eberlein, *Phys. Rev. A* **61**, 033614 (2000).
- [37] H. Pu, S. Raghavan, and N. P. Bigelow, *Phys. Rev. A* **63**, 063603 (2001).